

Electronic Supporting Information:

Selective fluoride encapsulated neutral tripodal receptor capsule: Solvatochromism and solvatomorphism

Sandeep Kumar Dey and Gopal Das*

Department of Chemistry, Indian Institute of Technology Guwahati, Assam, 781 03, India,.

Fax: +91-361-258-2349; Tel: +91-361-258-2313

E-mail: gdas@iitg.ernet.in

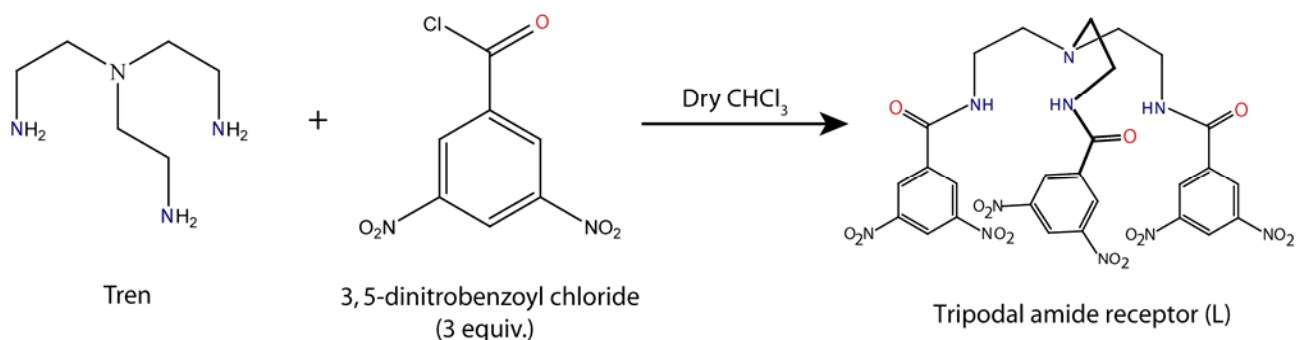
1.	Experimental section and characterization data of receptors L and CL	S-2
2.	X-ray crystallographic refinement details and table	S-7
3.	Fluoride binding study of receptor L (NMR, ESI-MS, FT-IR and crystal structures)	S-8
4.	TGA curves of crystals of fluoride complexes 1b and 1c	S-13
5.	Table for H-bond interactions of F ⁻ with L in complexes 1a , 1b and 1c	S-14
6.	¹ H NMR titration of L with TBAF and jobs plot	S-15
7.	¹⁹ F NMR spectra of TBAF in presence of L in DMSO- <i>d</i> ₆	S-17
8.	Anion binding study of control receptor CL	S-18
9.	UV/Vis titration curves of L with TBAF in various aprotic solvents	S-20
10.	UV/Vis titration curves of L and CL with protic solvents in presence of TBAF	S-22
11.	¹ H NMR spectra of L in presence of other halides	S-24
12.	¹ H NMR spectra of L in presence of oxoanions	S-25

Experimental Section:

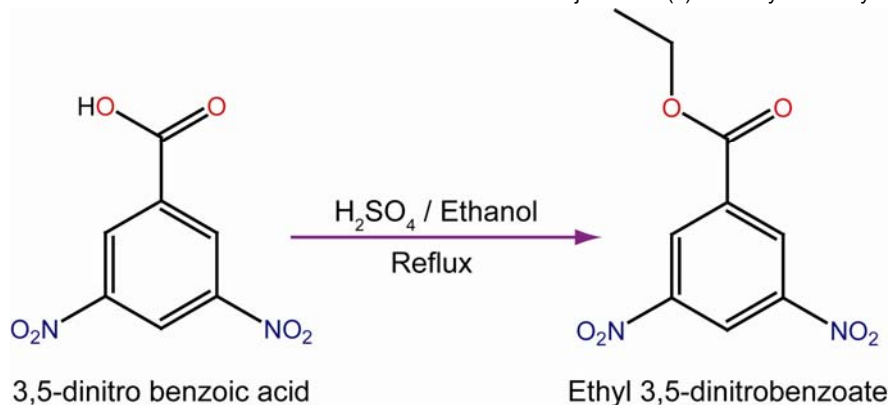
^1H and ^{13}C NMR spectra were recorded on a Varian FT-400 MHz spectrometer in $\text{DMSO-}d_6$ at 298 K. The IR spectra were recorded on a Perkin-Elmer-Spectrum One FT-IR spectrometer with KBr disks in the range $4000\text{-}450\text{ cm}^{-1}$. The absorption spectra were recorded on a Perkin-Elmer Lambda-25/35 UV/Visible spectrophotometer at 298 K and with a quartz cuvette (path length: 1 cm). All the tetrabutylammonium (TBA) salts used were purchased from Sigma-Aldrich, USA and were used as received. All solvents viz. CHCl_3 , DMSO, DMF, MeCN, Me_2CO , THF and dioxane were purchased from Spectrochem Ltd., India. Chemical shifts for ^1H and ^{13}C NMR were reported in parts per million (ppm), calibrated to the residual solvent peak set, with coupling constants reported in Hertz (Hz). The thermal analyses of the polymorphs were performed by using an SDTA 851 e TGA thermal analyzer (*Mettler Toledo*) with a heating rate of 10°C per min in a N_2 atmosphere. Optical micrograph images were taken in a *Zeiss-Axio Cam-M Rc* microscope fitted with a digital camera of air-dried crystals on glass micro slides.

Synthesis of receptors **L** and **CL**:

Tripodal amide-based receptor **L** is synthesized by the reaction of tris(2-aminoethyl)amine with three equivalents of 3,5-dinitrobenzoyl chloride in presence of triethylamine in dry chloroform at RT. After stirring overnight, the reaction mixture is filtered and the precipitate is washed with plenty of water and methanol to remove the triethylammonium chloride and dried under vacuum to yield the light brown solid of **L** (Yield = 73%). The ligand has been characterized by NMR, FT-IR, ESI-MS and single crystal X-ray analyses. Single crystals of **L** suitable for X-ray diffraction analysis are grown from DMSO at RT.



Scheme S1. Synthesis of tripodal tris-(amide) receptor **L**.



Scheme S2. Synthesis of control receptor **CL**.

Characterization of receptor L:

m.p. = 252 °C; $^1\text{H-NMR}$ (400 MHz, $\text{DMSO-}d_6$) δ 2.79 (s, 6H, $-\text{NCH}_2$), 3.43 (s, 6H, $-\text{OCH}_2$), 8.88 (s, 3H, ArH_{para}), 8.91 (s, 6H, $\text{ArH}_{\text{ortho}}$), 9.12 (s, 3H, $-\text{NH}$); $^{13}\text{C NMR}$ (100 MHz, $\text{DMSO-}d_6$): δ 45.73 ($\times 3\text{C}$, $-\text{NCH}_2$), 53.08 ($\times 3\text{C}$, $-\text{OCH}_2$), 120.58 ($\times 3\text{C}$, ArH), 127.35 ($\times 3\text{C}$, ArH), 137.06 ($\times 3\text{C}$, ArH), 148.01 ($\times 3\text{C}$, ArH), 162.20 ($\times 3\text{C}$, C=O); ESI-mass: 729.15 [$\text{M}+1$]; FT-IR ($\nu \text{ cm}^{-1}$): 1670 (C=O), 3428 (N-H).

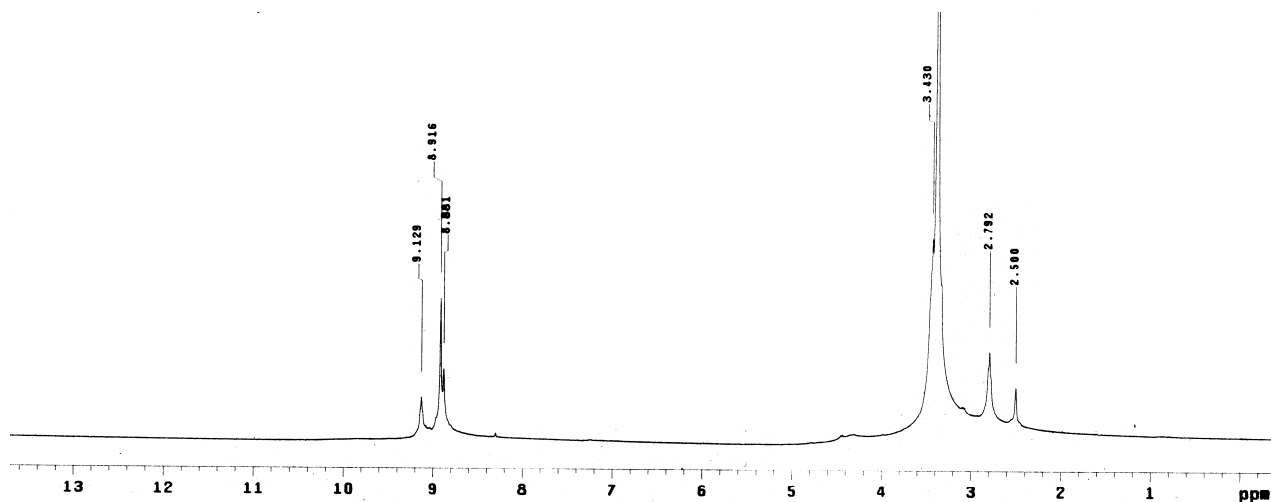


Figure S1. $^1\text{H NMR}$ spectrum of **L** in $\text{DMSO-}d_6$ at 298 K.

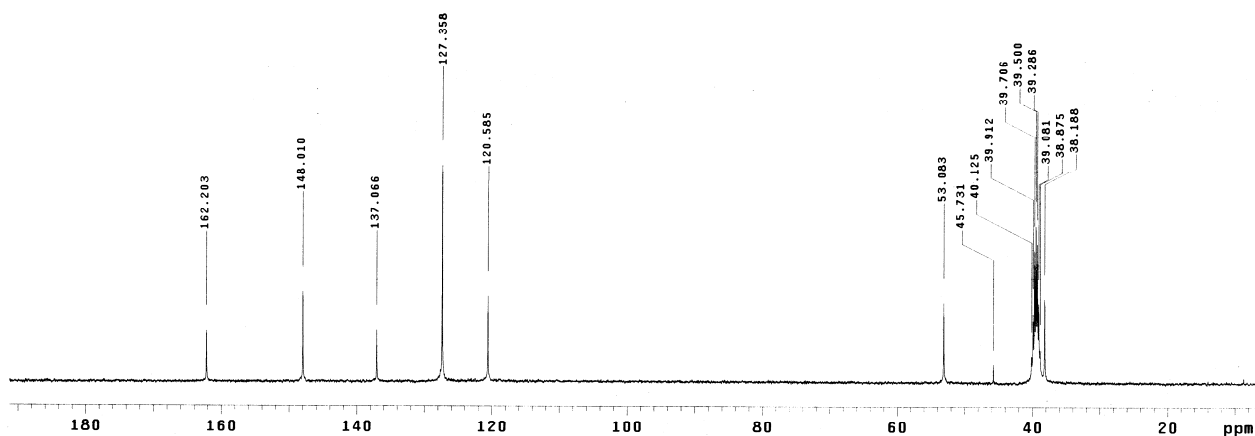


Figure S2. ^{13}C NMR spectrum of **L** in $\text{DMSO-}d_6$ at 298 K.

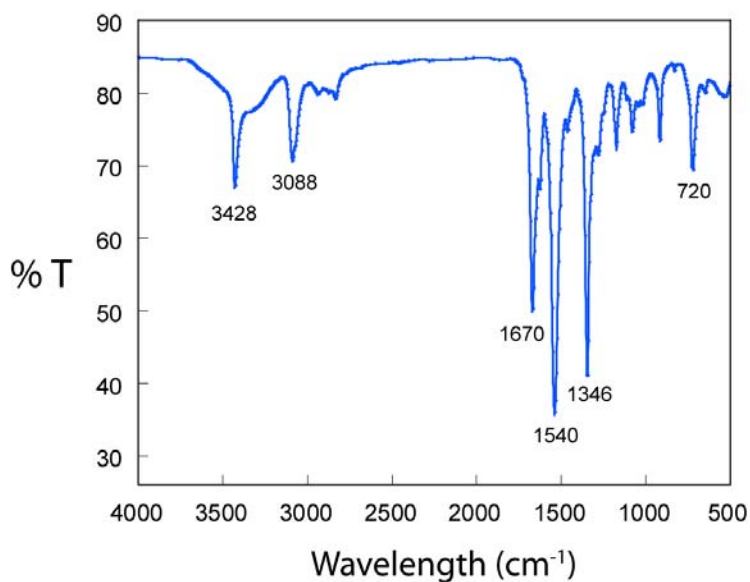


Figure S3. FT-IR spectrum of **L** recorded in KBr pellet.

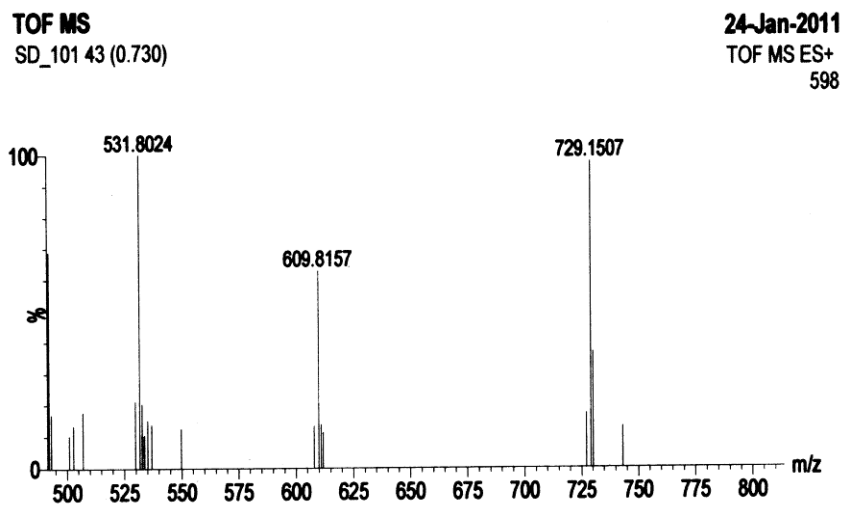


Figure S4. ESI-mass spectrum of **L** recorded in acetonitrile (MeCN) at 298 K showing $m/z = 729.15$ corresponds to $[\text{M}+1]$.

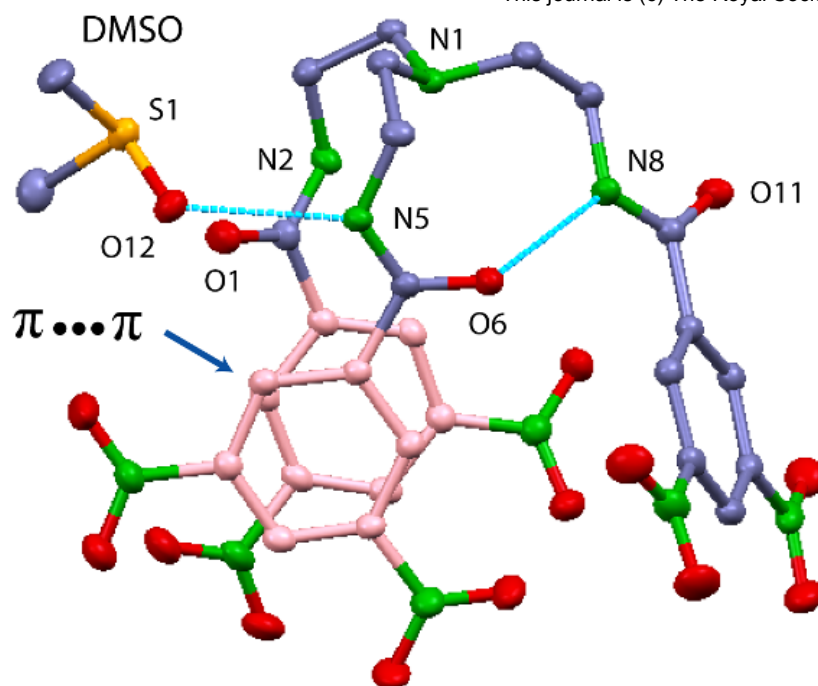


Figure S5. Thermal ellipsoid plot (30% probability) of receptor **L** depicting the formation of various intramolecular H-bonds (Aryl rings involved in $\pi \cdots \pi$ stacking are coloured as pink).

Characterization of control receptor CL:

$^1\text{H-NMR}$ (400 MHz, CDCl_3) δ 1.37 (t, 3H, $-\text{CH}_3$), 4.41 (q, 2H, $-\text{CH}_2$), 9.04 (s, 2H, ArH_{ortho}), 9.09 (s, 1H, ArH_{para}); $^{13}\text{C NMR}$ (100 MHz, CDCl_3): δ 14.18 ($\times 1\text{C}$, $-\text{CH}_3$), 62.97 ($\times 1\text{C}$, $-\text{CH}_2$), 122.26 ($\times 1\text{C}$, ArH), 129.38 ($\times 1\text{C}$, ArH), 134.07 ($\times 1\text{C}$, ArH), 148.58 ($\times 1\text{C}$, ArH), 162.46 ($\times 1\text{C}$, C=O).

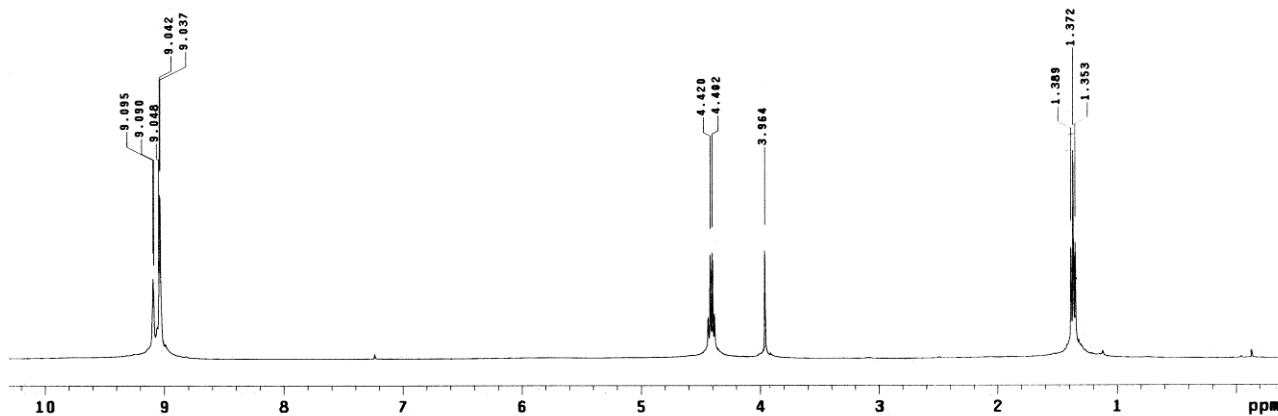


Figure S6. $^1\text{H NMR}$ spectrum of **CL** recorded in CDCl_3 at 298 K.

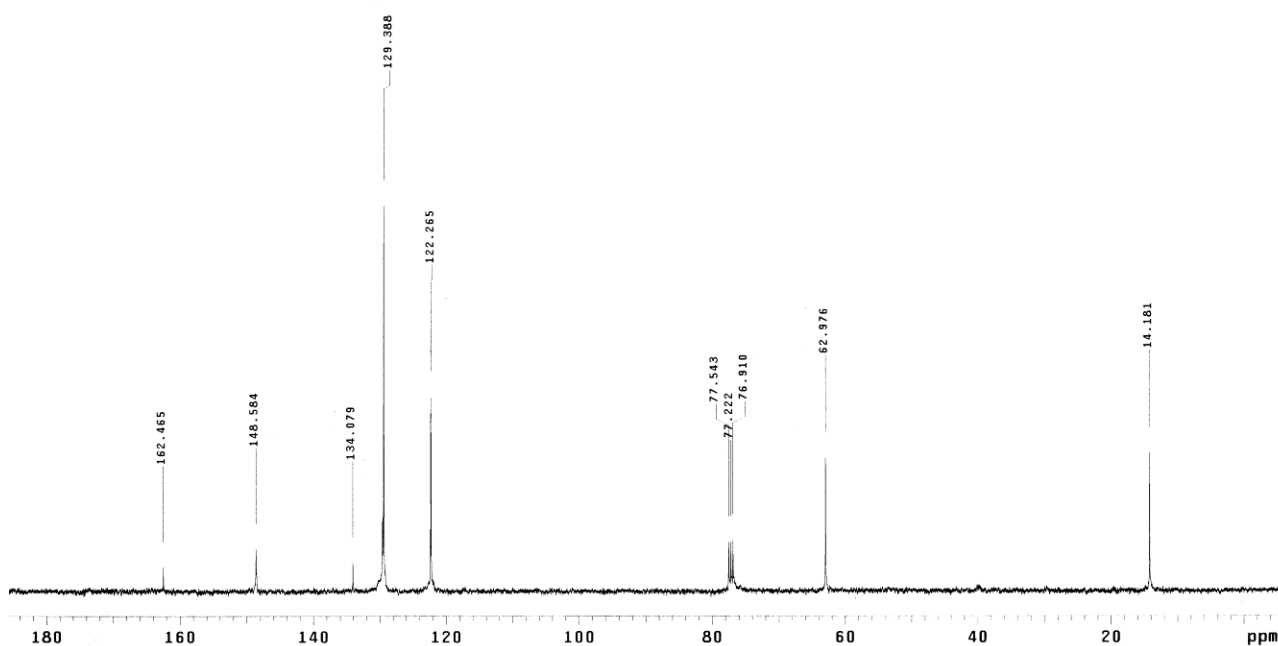


Figure S7. $^{13}\text{C NMR}$ spectrum of **CL** recorded in CDCl_3 at 298 K.

Crystallographic Refinement Details:

The crystallographic data and details of data collection for receptor **L** and complexes **1a**, **1b** and **1c** are given in Table S1. In each case, a crystal of suitable size was selected from the mother liquor and immersed in silicone oil, then mounted on the tip of a glass fibre and cemented using epoxy resin. Intensity data for the crystals were collected Mo-K α radiation ($\lambda = 0.71073\text{\AA}$) at 298(2) K, with increasing ω (width of 0.3° per frame) at a scan speed of 6 s/ frame on a Bruker SMART APEX diffractometer equipped with CCD area detector. The data integration and reduction were processed with SAINT¹ software. An empirical absorption correction was applied to the collected reflections with SADABS.² The structures were solved by direct methods using SHELXTL³ and were refined on F^2 by the full-matrix least-squares technique using the SHELXL-97 program package.⁴ Graphics are generated using MERCURY 1.4.⁵ In all cases, non-hydrogen atoms are treated anisotropically. Wherever possible, the hydrogen atoms are located on a difference Fourier map and refined. In other cases, the hydrogen atoms are geometrically fixed. However, we were unable to locate the hydrogen atoms of lattice water in **1a** from the difference Fourier map. PLATON/SQUEEZE⁶ was performed to refine the host framework in **1c** along with the entrapped fluoride ion and TBA cation by excluding the disordered solvent electron densities. These calculations amount to 130 electrons per molecule and may be attributed to three disordered THF molecules, further supported by the TGA curve of crystals of **1c**.

Table S1. Crystallographic details of data collection for receptor **L** and complexes **1a**, **1b** and **1c**.

Parameters	L	1a	1b	1c
Empirical formula	C ₂₉ H ₃₀ N ₁₀ O ₁₆ S	C ₄₃ H ₆₀ FN ₁₁ O ₁₆	C ₄₆ H ₆₇ FN ₁₂ O ₁₆	C ₄₃ H ₆₀ FN ₁₁ O ₁₅
Formula weight	806.70	1006.02	1063.12	990.02
Crystal system	Triclinic	Monoclinic	Triclinic	Monoclinic
Space group	<i>P</i> -1	<i>P</i> ₂ / <i>c</i>	<i>P</i> -1	<i>P</i> ₂ / <i>c</i>
<i>a</i> /Å	11.2942(3)	16.129(3)	10.0759(3)	10.0293(9)
<i>b</i> /Å	12.4744(4)	15.781(2)	16.7929(6)	33.293(3)
<i>c</i> /Å	12.8671(4)	25.393(4)	16.8986(5)	19.4982(17)
α /°	84.723(2)	90.00	79.197(2)	90.00
β /°	79.650(3)	127.592(9)	78.461(3)	90.382(6)
γ /°	88.404(2)	90.00	89.753(2)	90.00
<i>V</i> /Å ³	1775.65(9)	5121.4(15)	2750.23(16)	6510.4(10)
<i>Z</i>	2	4	2	4
<i>D</i> _c /g cm ⁻³	1.509	1.305	1.284	1.010
μ Mo K α /mm ⁻¹	0.180	0.103	0.100	0.079
<i>T</i> /K	298(2)	298(2)	298(2)	298(2)
2 θ max.	28.29	24.89	28.39	24.87
Total reflections	13679	35440	29276	73179
Unique reflections	8734	8854	13732	11177
Observed reflections	7605	7719	11770	9245
Parameters refined	520	644	683	635
<i>R</i> ₁ ; w <i>R</i> ₂ (all data)	0.0508; 0.1510	0.0603; 0.2034	0.0693; 0.1841	0.0814; 0.1952
GOF (<i>F</i> ²)	0.911	1.008	1.011	1.018

Fluoride binding study of receptor L:

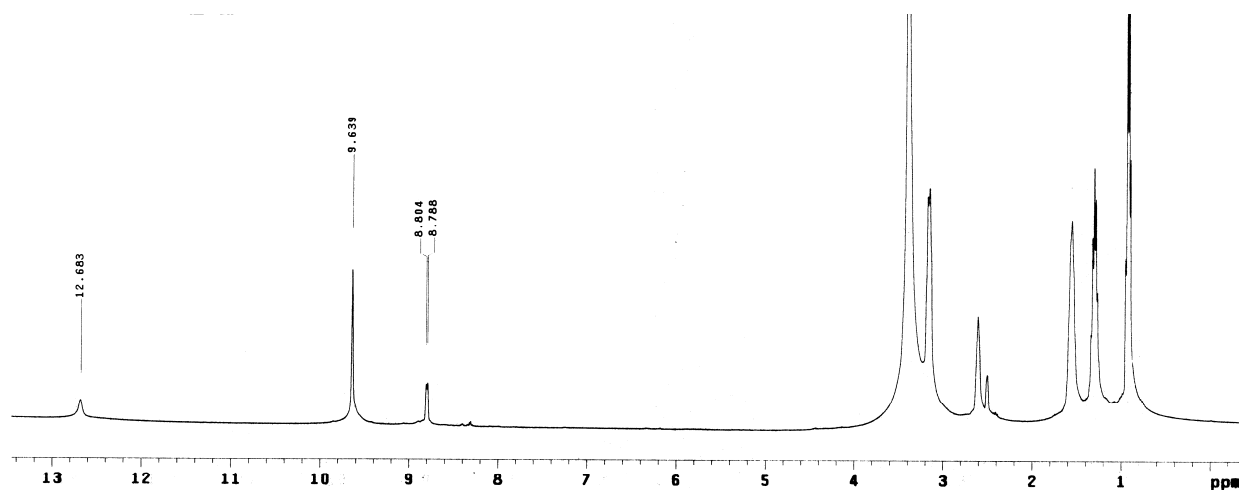


Figure S8. ^1H NMR spectrum of **L** in $\text{DMSO-}d_6$ upon addition of equivalent amount of TBAF at 298 K. (The appreciable downfield shift of aromatic -CH proton signal ($\Delta\delta = 0.72$ ppm) indicates the active participation of the aryl -CH protons in the F^- binding event in solution. Nitro group substitutions in the aryl terminals increases the aromatic CH acidity which facilitate these $\text{C-H}\cdots\text{F}^-$ interactions to a considerable extent).

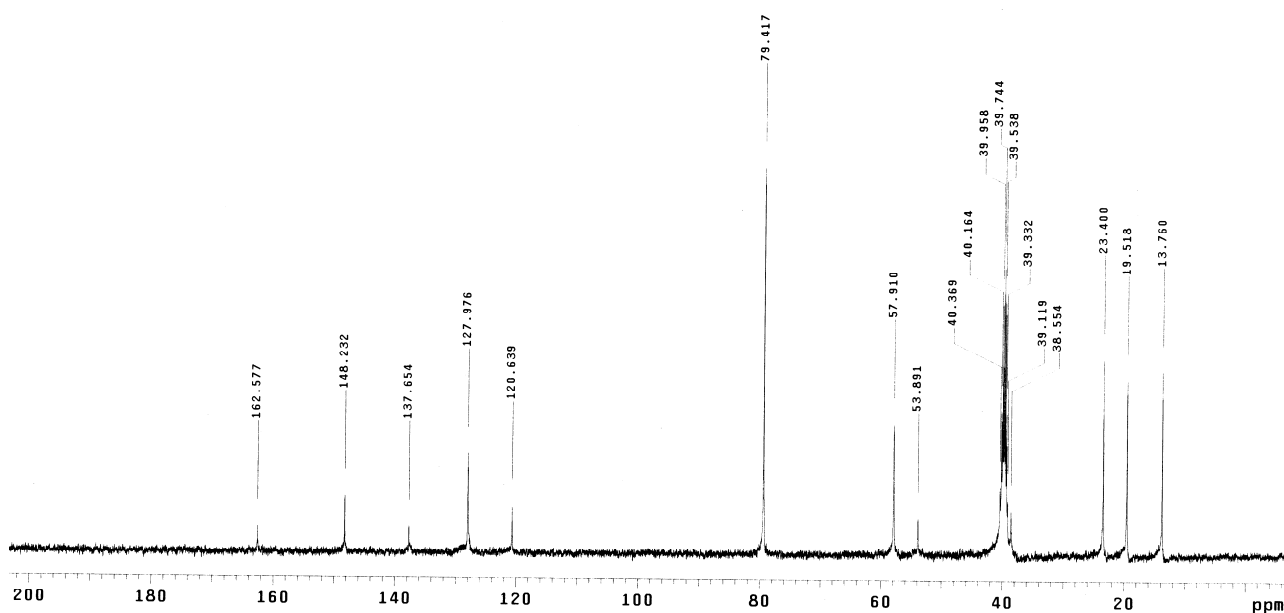


Figure S9. ^{13}C NMR spectrum of **L** in $\text{DMSO-}d_6$ upon addition of equivalent amount of TBAF at 298 K.

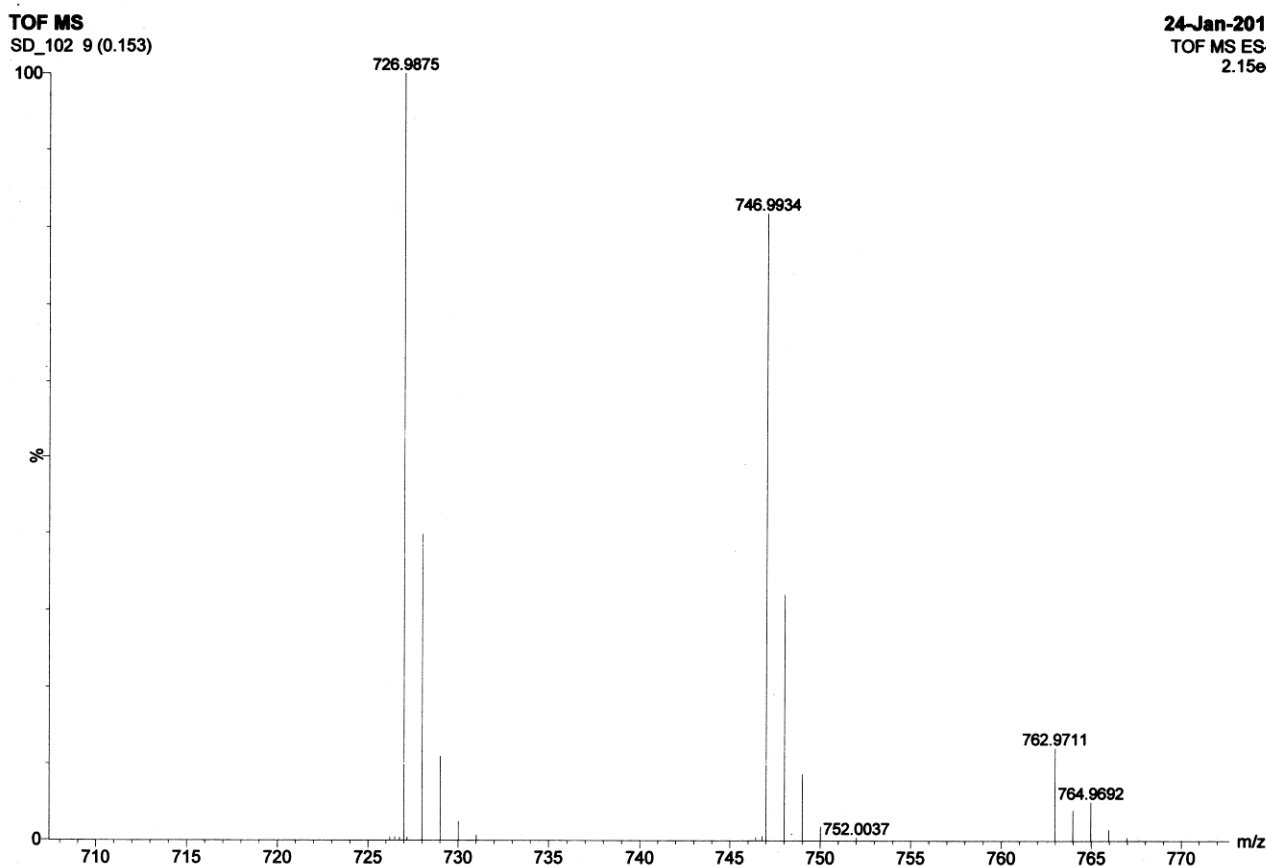


Figure S10. ESI-mass spectrum of **L** in presence of excess TBAF in acetonitrile (MeCN) showing $m/z = 746.99$ for the fluoride encapsulated receptor capsule.

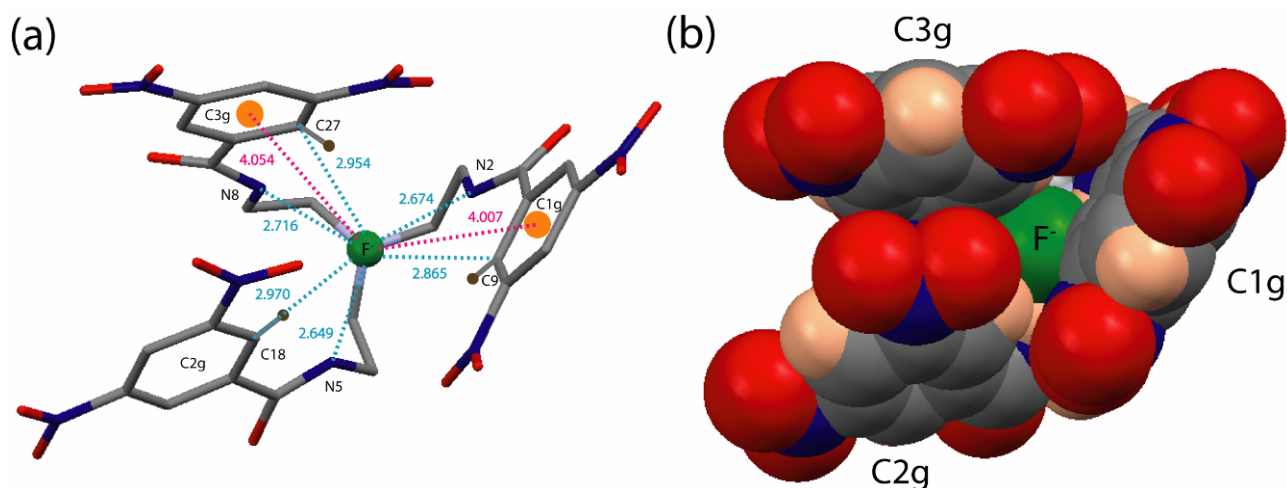


Figure S11. (a) Crystal structure of **1b** showing encapsulation of F^- (green, ball and stick) inside the tripodal cavity where blue dotted lines represent the $(D-H)\cdots F^-$ interactions and pink dotted lines depict $F^- \cdots \pi$ interactions; (b) Spacefill representation depicting the formation of F^- encapsulated neutral receptor capsule in **1b**. TBA cation and lattice DMF molecule are omitted for clarity.

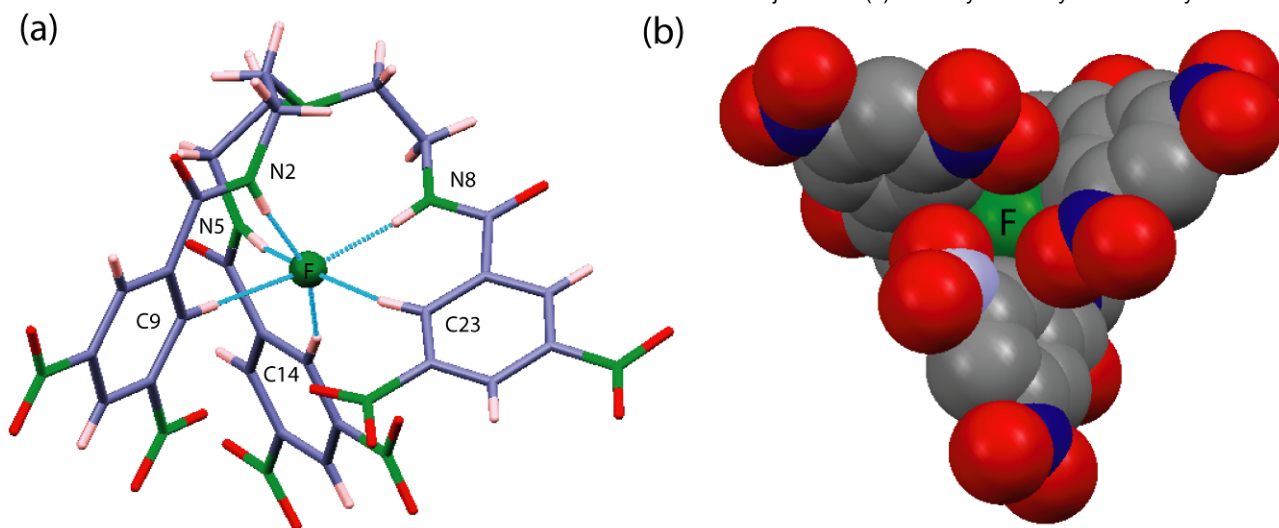


Figure S12. (a) Crystal structure of **1c** showing encapsulation of F^- (green, ball and stick) inside the tripodal cavity where blue dotted lines represent the $(D-H)\cdots F^-$ interactions; (b) Spacefill representation depicting the formation of F^- encapsulated neutral receptor capsule in **1c**. TBA cation and lattice THF molecules are omitted for clarity.

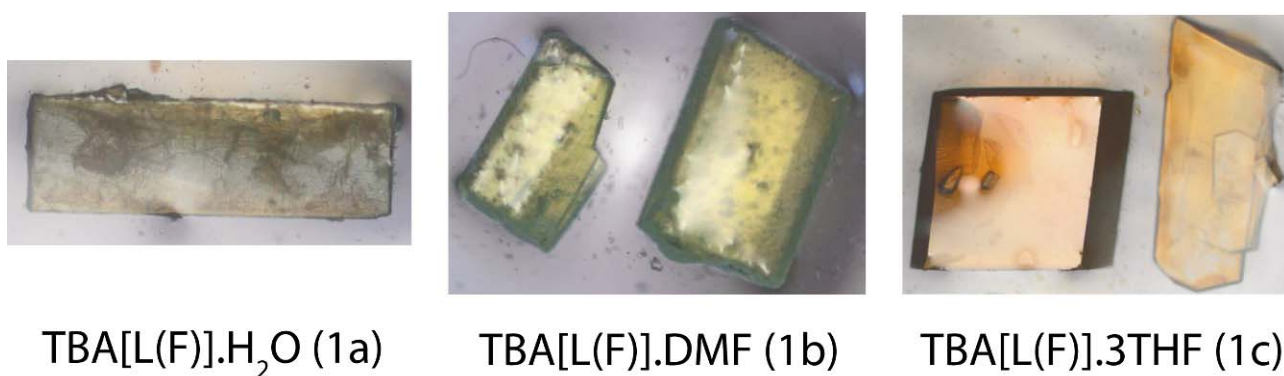


Figure S13. Optical micrograph images of crystals **1a**, **1b** and **1c**.

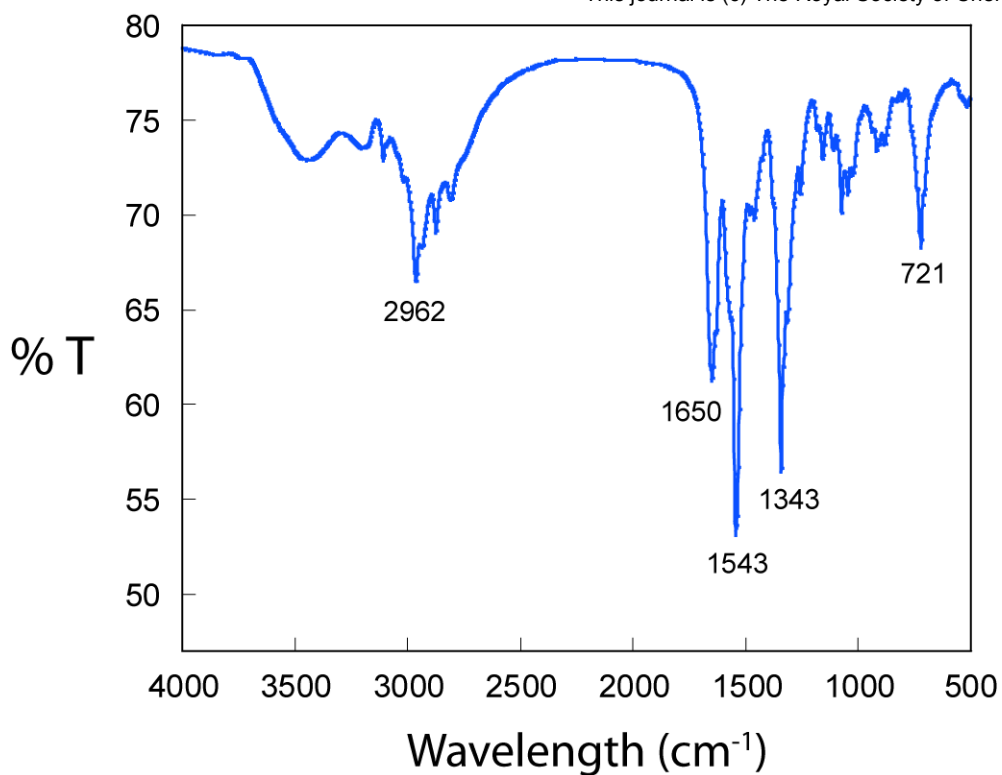


Figure S14. FT-IR spectrum of solvatomorph **1a** recorded in KBr pellet.

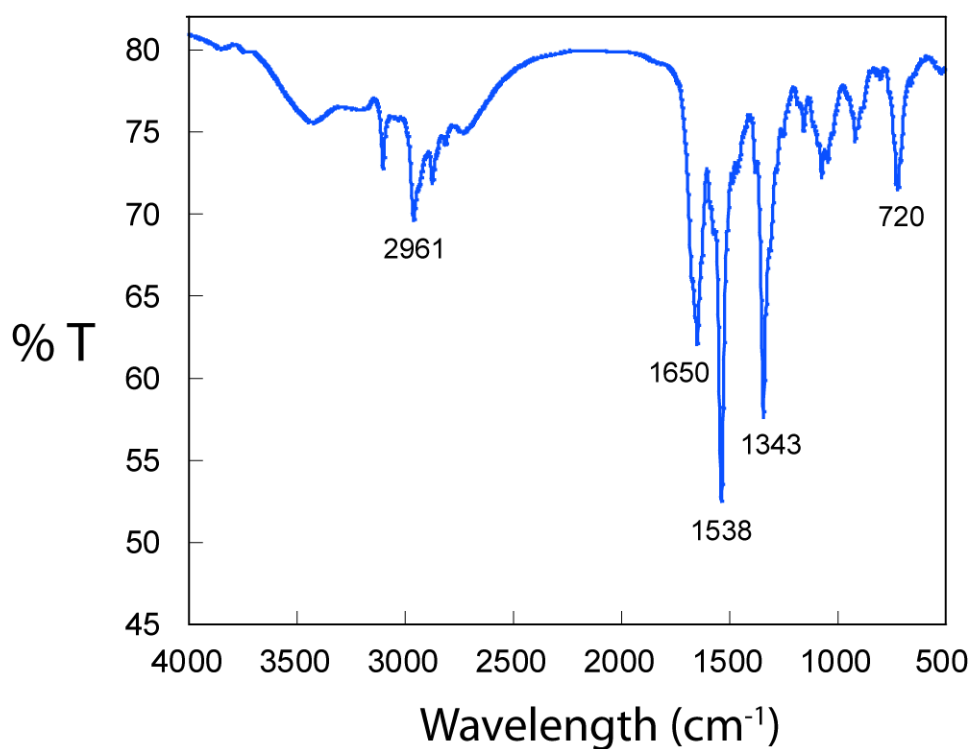


Figure S15. FT-IR spectrum of solvatomorph **1b** recorded in KBr pellet.

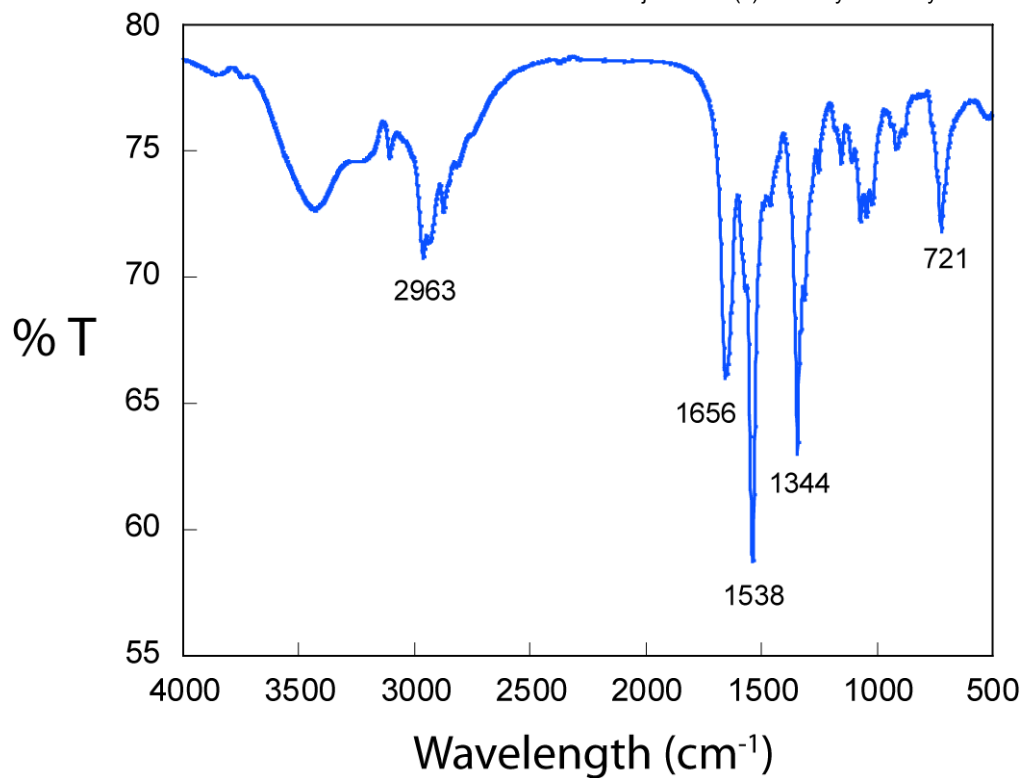


Figure S16. FT-IR spectrum of solvatomorph **1c** recorded in KBr pellet.

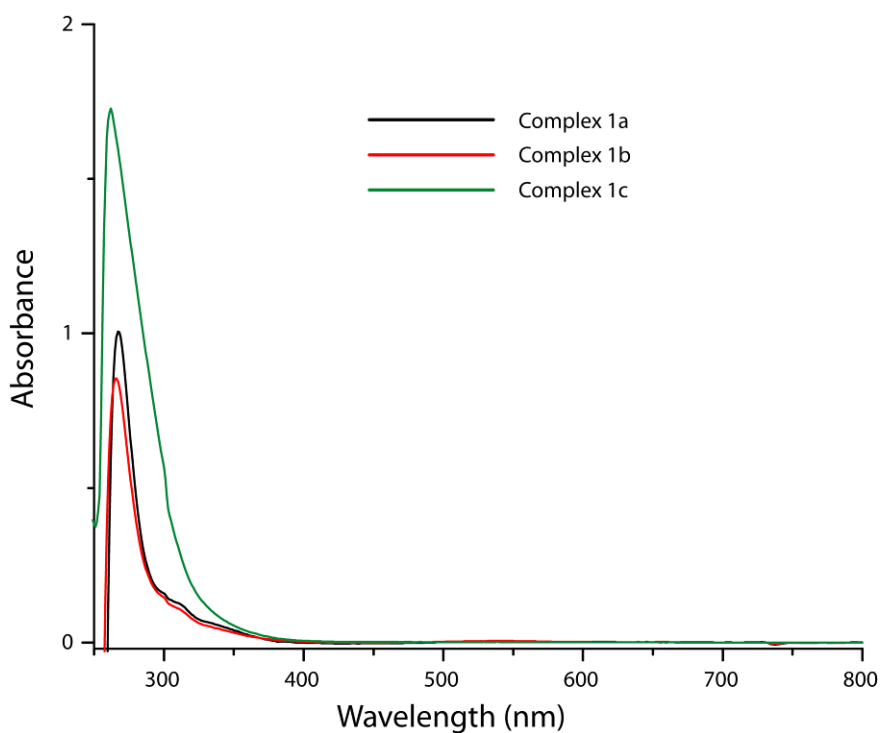


Figure S17. Solid-state UV/Vis spectra of solvatomorphs **1a**, **1b** and **1c**.

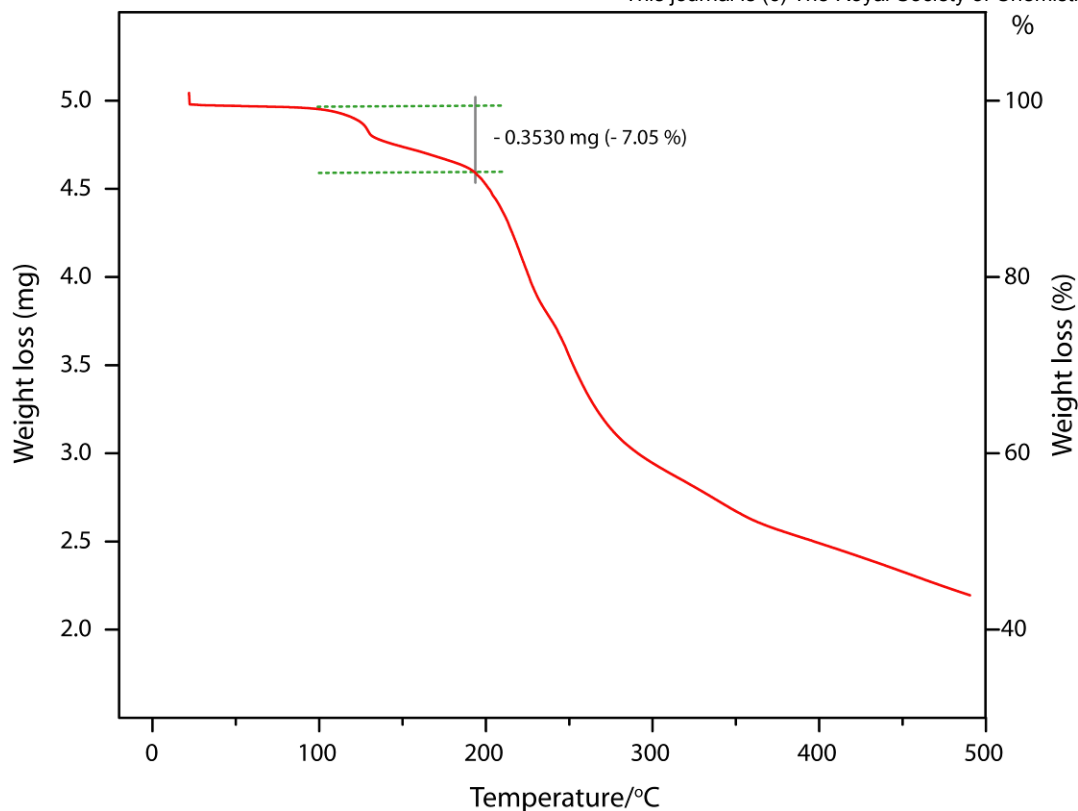


Figure S18. Thermogravimetric curve of complex TBA[L(F)]•DMF (**1b**) at a heating rate of 10 °C showing a weight loss of ~ 7 % equivalent to one DMF molecule.

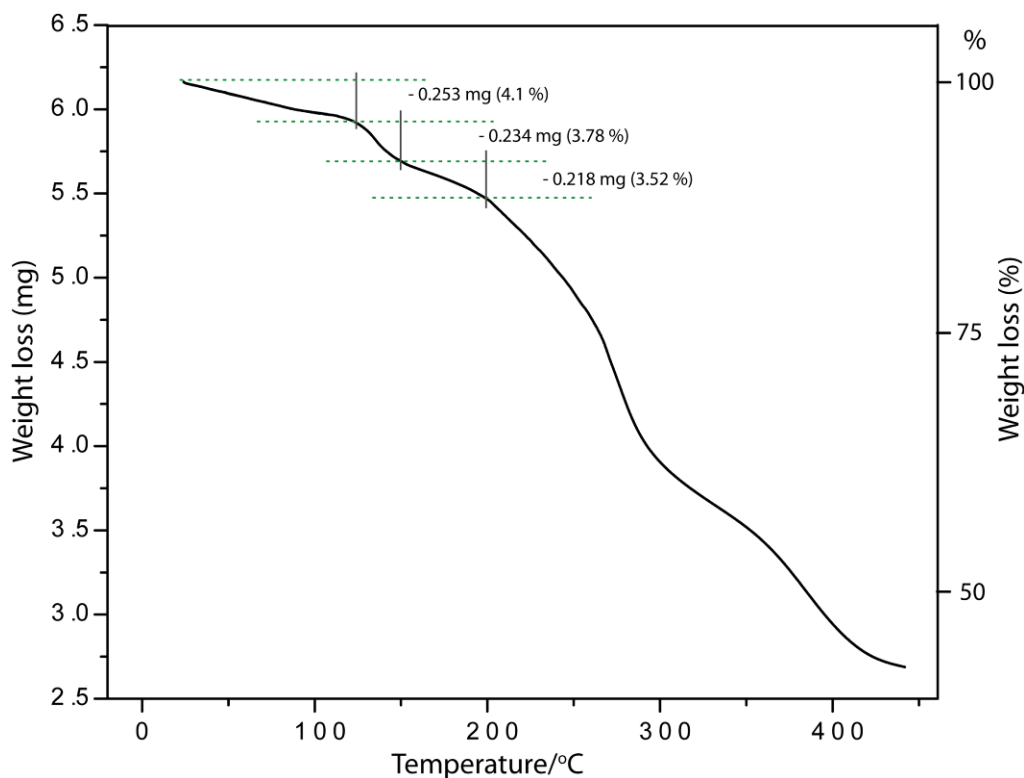


Figure S19. Thermogravimetric curve of complex TBA[L(F)]•3THF (**1c**) at a heating rate of 10 °C showing three step weight loss of lattice THF molecules.

Table S2. H-bonding interactions of F⁻ with receptor **L** in complexes **1a**, **1b** and **1c**.

Complex 1a , TBA[L (F)]•H ₂ O			
D-H•••F	<i>d</i> (H•••F)/Å	<i>d</i> (D•••F)/Å	<D-H•••F/ ^o
N2-H•••F1	1.84(2)	2.683(4)	165(2)
N5-H•••F1	1.87(2)	2.718(3)	167(2)
N8-H•••F1	1.88(2)	2.718(3)	163(2)
C9-H9•••F1	2.13(2)	3.012(3)	156(2)
C18-H18•••F1	2.14(2)	2.970(4)	147(2)
C27-H27•••F1	2.10(2)	3.012(4)	164(2)
Complex 1b , TBA[L (F)]•DMF			
D-H•••F	<i>d</i> (H•••F)/Å	<i>d</i> (D•••F)/Å	<D-H•••F/ ^o
N2-H•••F1	1.87(1)	2.674(3)	154(2)
N5-H•••F1	1.83(2)	2.649(3)	156(2)
N8-H•••F1	1.95(1)	2.716(3)	147(2)
C9-H9•••F1	2.25(2)	2.865(4)	122(2)
C18-H18•••F1	2.18(1)	2.970(3)	142(2)
C27-H27•••F1	2.38(1)	2.954(3)	119(2)
Complex 1c , TBA[L (F)]•3THF			
D-H•••F	<i>d</i> (H•••F)/Å	<i>d</i> (D•••F)/Å	<D-H•••F/ ^o
N2-H•••F1	1.82(2)	2.674(4)	169(2)
N5-H•••F1	1.83(2)	2.687(4)	170(3)
N8-H•••F1	1.89(2)	2.755(4)	173(2)
C9-H9•••F1	2.09(2)	2.984(5)	161(3)
C18-H18•••F1	2.08(2)	2.985(5)	161(3)
C27-H27•••F1	2.14(2)	3.027(5)	158(3)

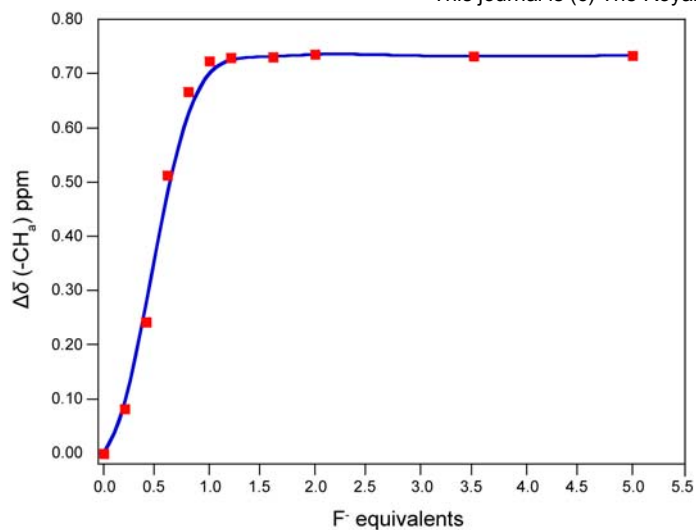


Figure S20. Change in chemical shift of $-CH$ (coordinating ortho protons) resonance of **L** (20 mM) with increasing amounts of TBAF in $DMSO-d_6$ at 298 K giving $\log K > 7.0$ (error limit $< 15\%$).

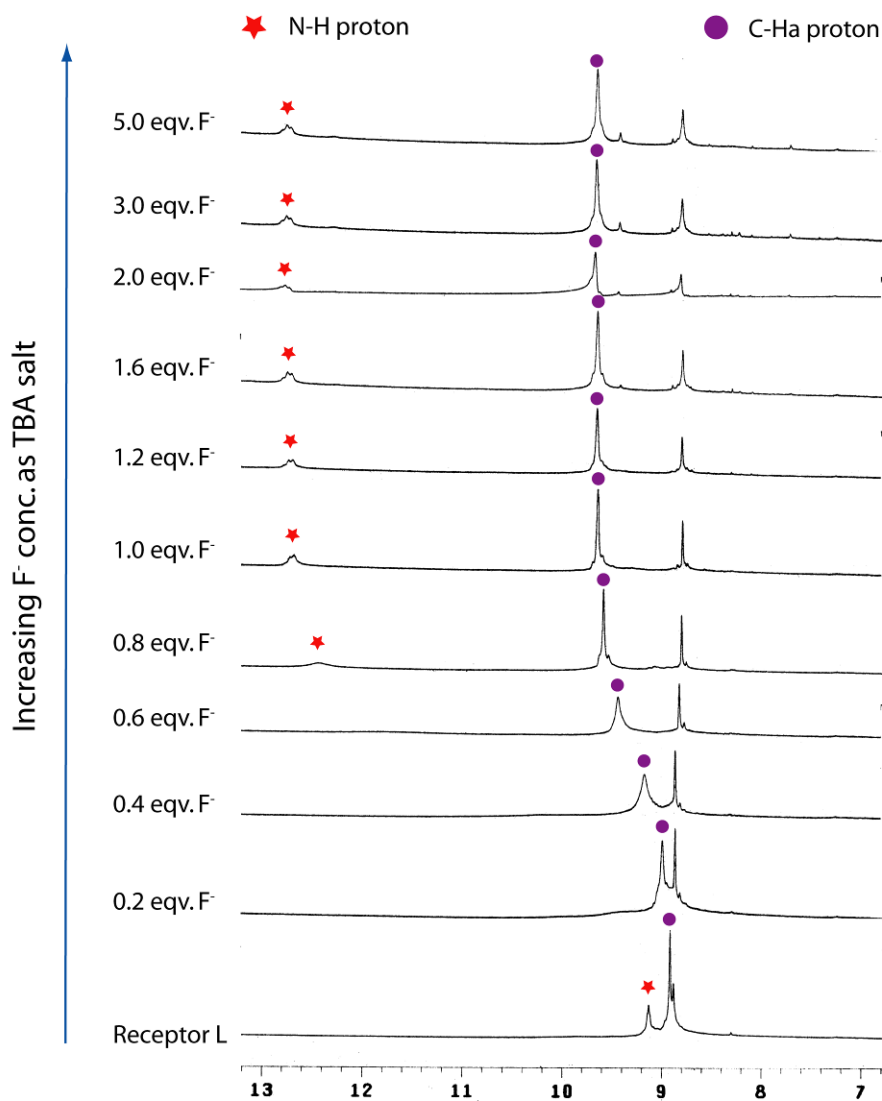


Figure S21. Partial 1H NMR spectra showing the titration of **L** in $DMSO-d_6$ upon gradual addition of TBAF at 298 K.

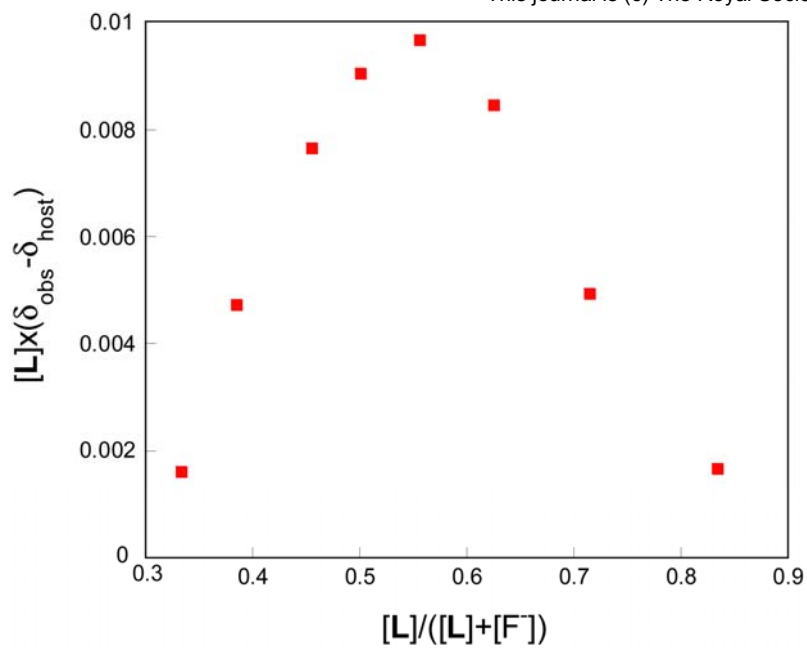


Figure S22. Jobs plot for **L** with TBAF in DMSO- d_6 at 298 K.

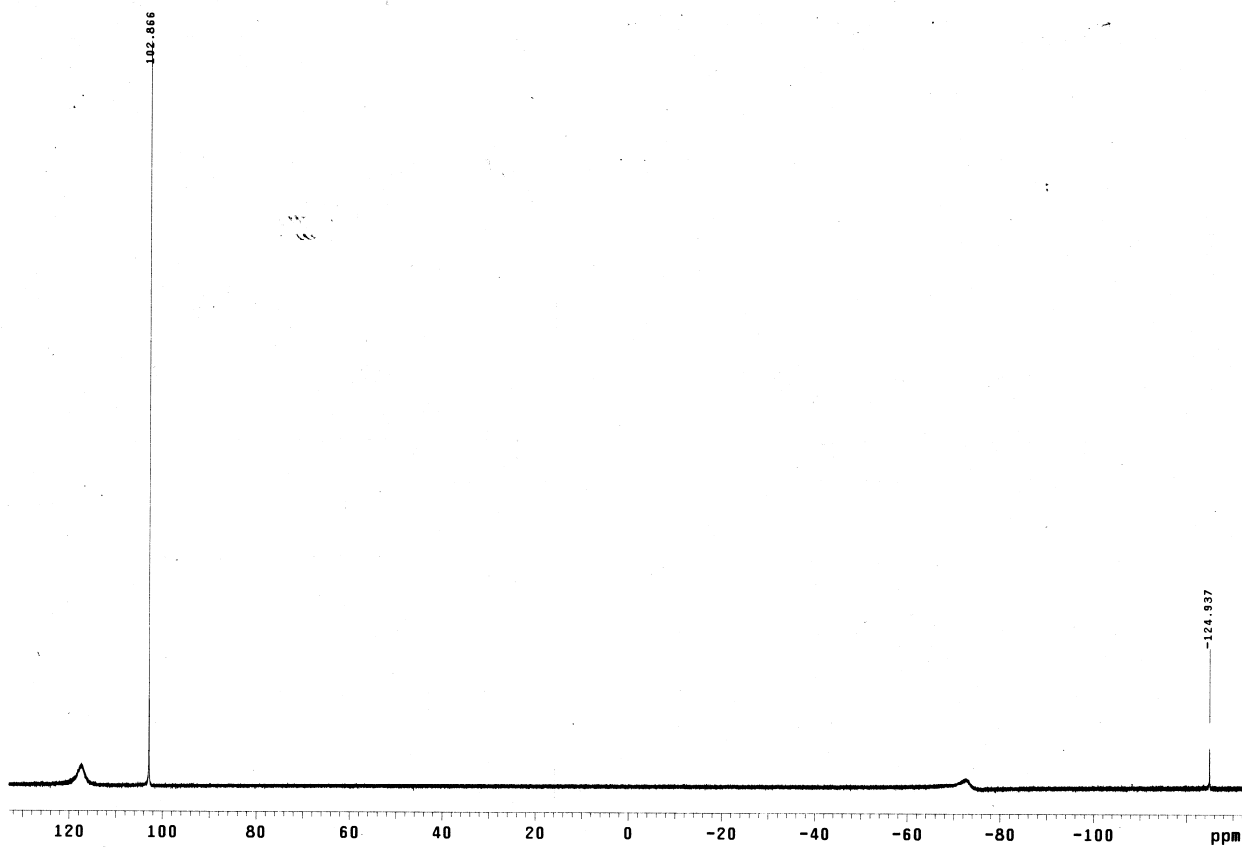


Figure S23. ^{19}F NMR spectrum of TBAF in DMSO- d_6 upon addition of equivalent amount of **L**. Hexafluorobenzene was used as an internal standard.

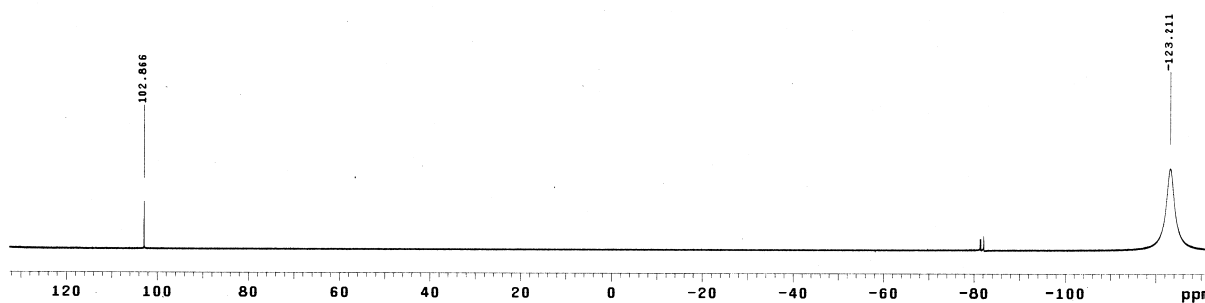


Figure S24. ^{19}F NMR spectrum of TBAF in $\text{DMSO-}d_6$. Hexafluorobenzene was used as an internal standard.

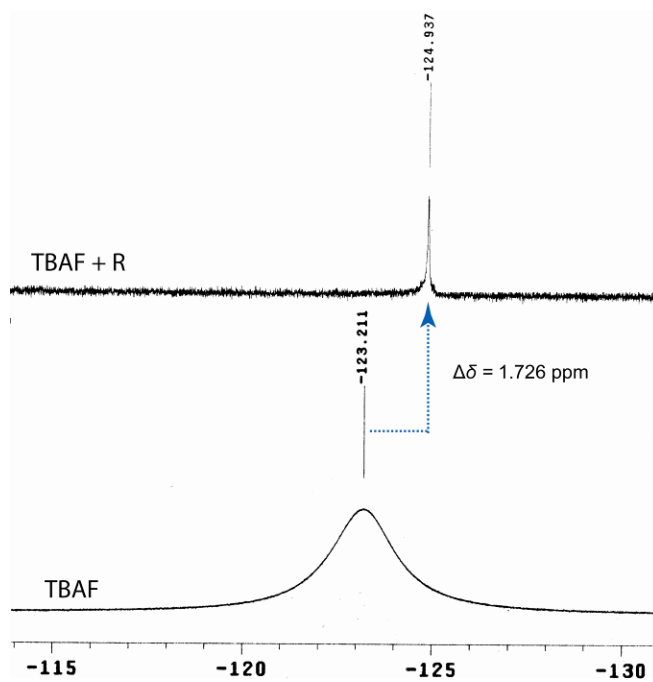


Figure S25. Partial ^{19}F NMR spectrum of TBAF in $\text{DMSO-}d_6$ and upfield shift of F^- resonance upon addition of **L**.

Anion binding study of control receptor CL_2

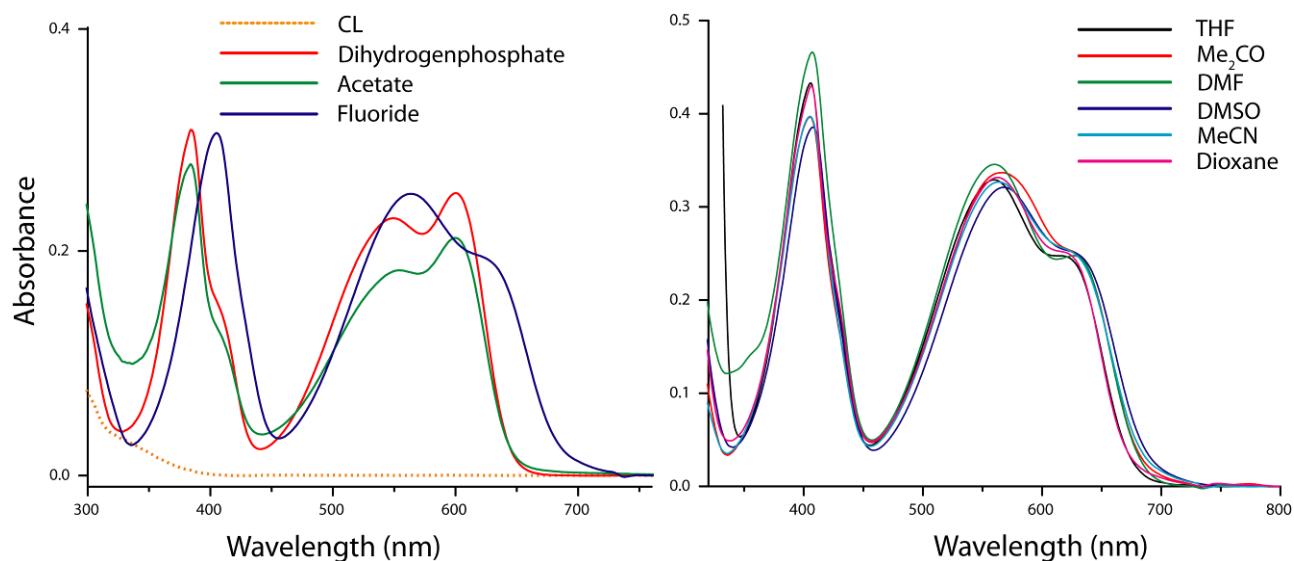


Figure S26. Changes in the UV/Vis spectrum of **CL** in acetonitrile solution upon addition of TBA salts of strongly basic anions such as, fluoride, acetate and dihydrogenphosphate anions (left) and no observable changes have been observed in the UV/Vis spectrum of **CL** in various aprotic solvents upon addition of TBA salt of F^- (right).



Figure S27. Colour changes observed with the addition of excess anions to acetonitrile solutions of **CL**.

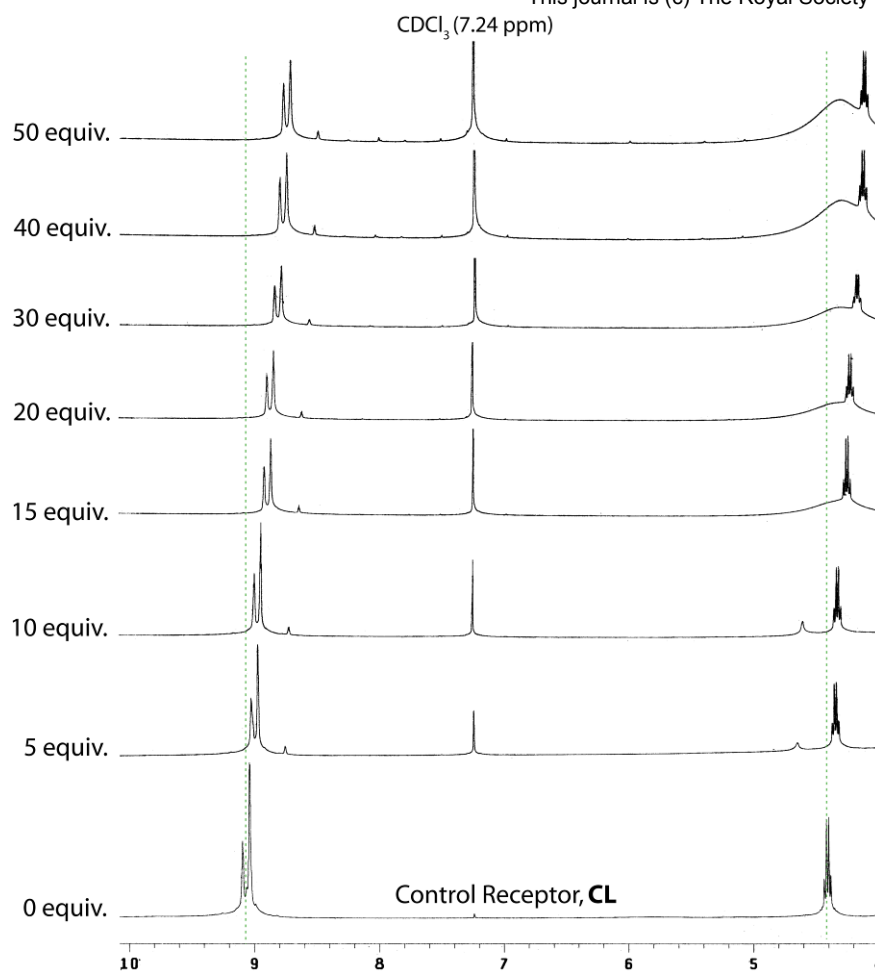


Figure S28. Partial ^1H NMR spectra showing the titration of **CL** in CDCl_3 upon increasing addition of TBAF at 298 K.

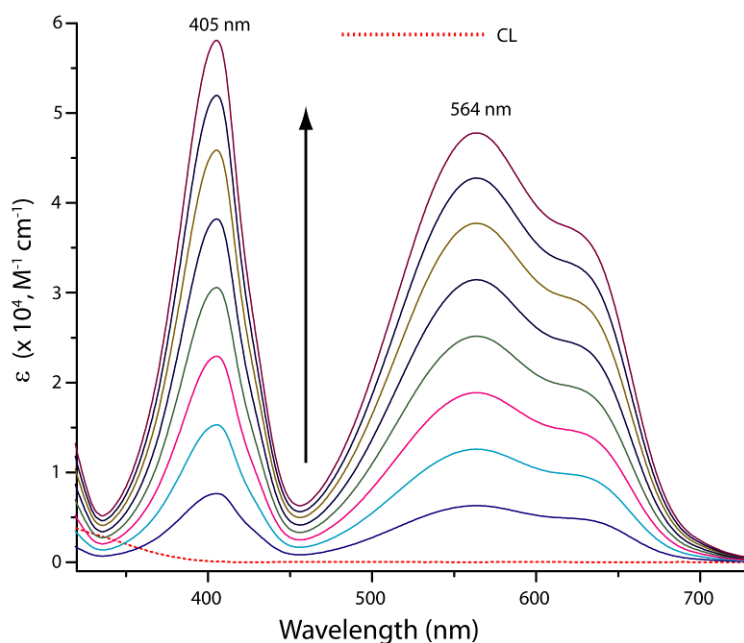


Figure S29. UV-Vis absorption titration of **CL** ($10\ \mu\text{M}$) in acetonitrile (MeCN) upon addition of standard fluoride solution ($10\ \text{mM}$).

UV/Vis titration curves of L with TBAF in various aprotic solvents:

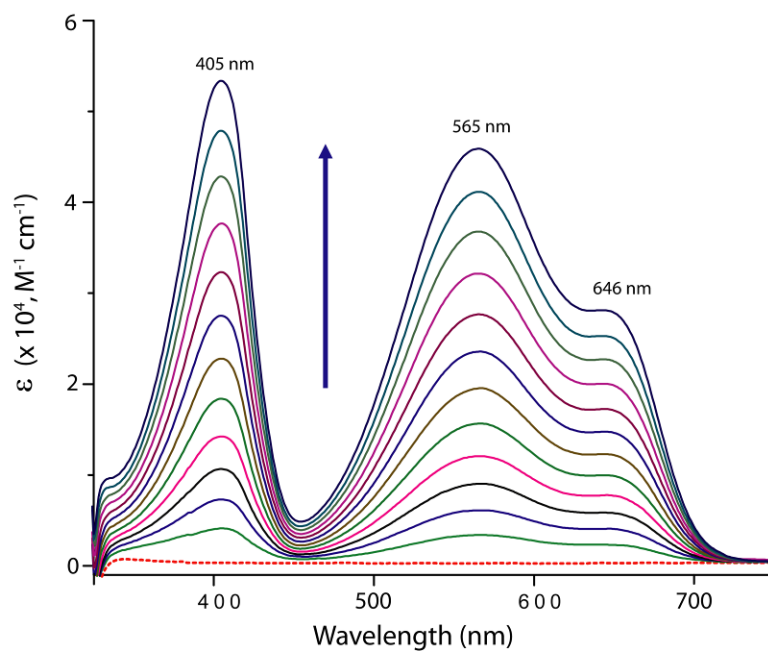


Figure S30. UV-Vis absorption titration of L (10 μM) in acetone upon addition of standard fluoride solution (10 mM).

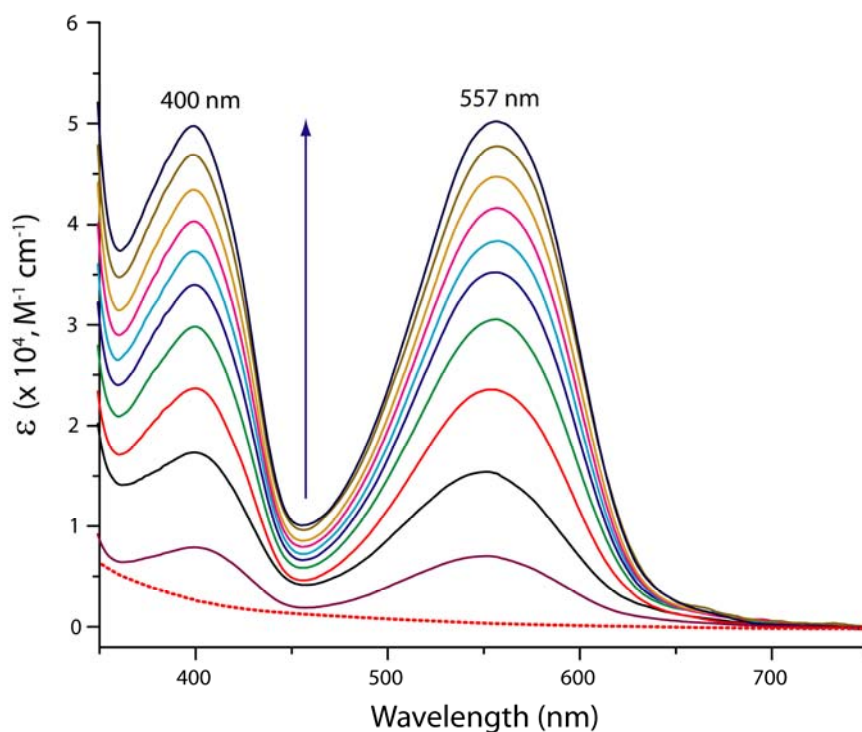


Figure S31. UV-Vis absorption titration of L (10 μM) in THF upon addition of standard fluoride solution (10 mM).

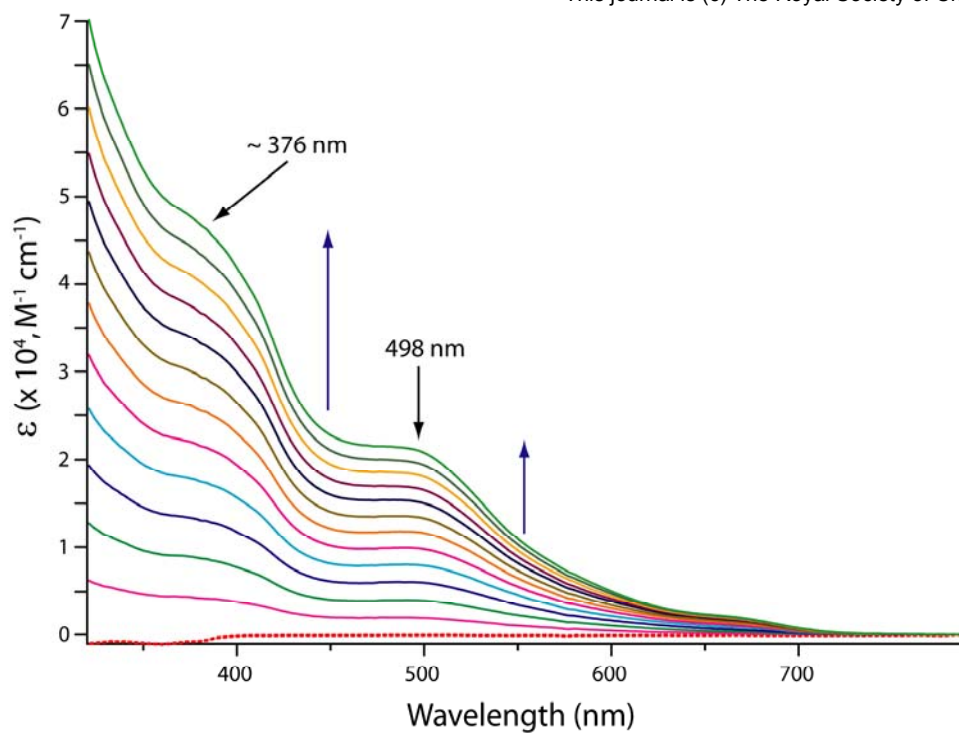


Figure S32. UV-Vis absorption titration of **L** (10 μM) in acetonitrile (MeCN) upon addition of standard fluoride solution (10 mM).

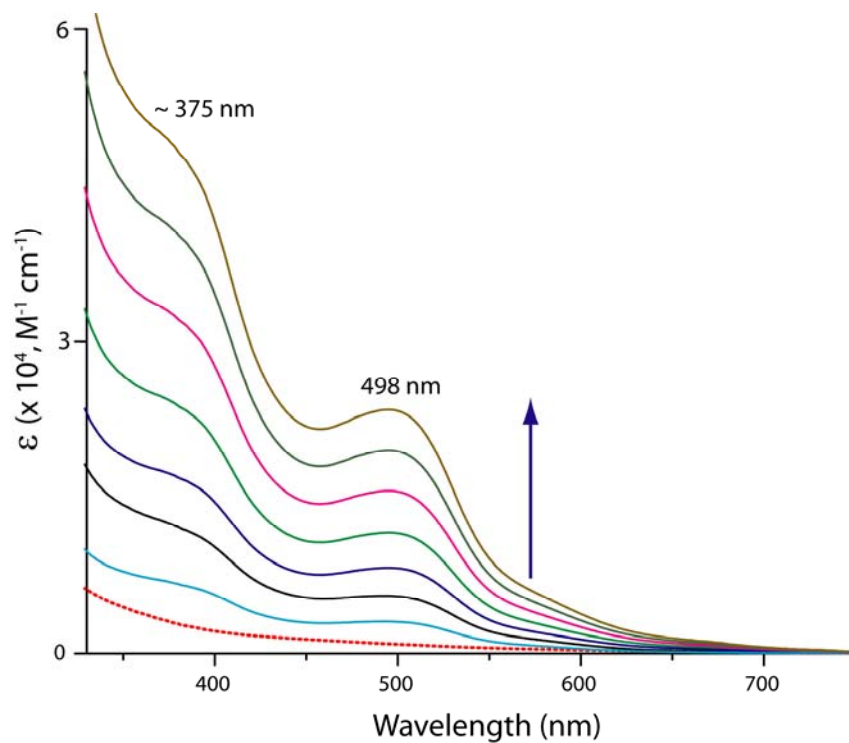


Figure S33. UV-Vis absorption titration of **L** (10 μM) in dioxane upon addition of standard fluoride solution (10 mM).

UV/Vis titration curves of L and CL with protic solvents (MeOH and water) in presence of excess TBAF in dry aprotic solvents:

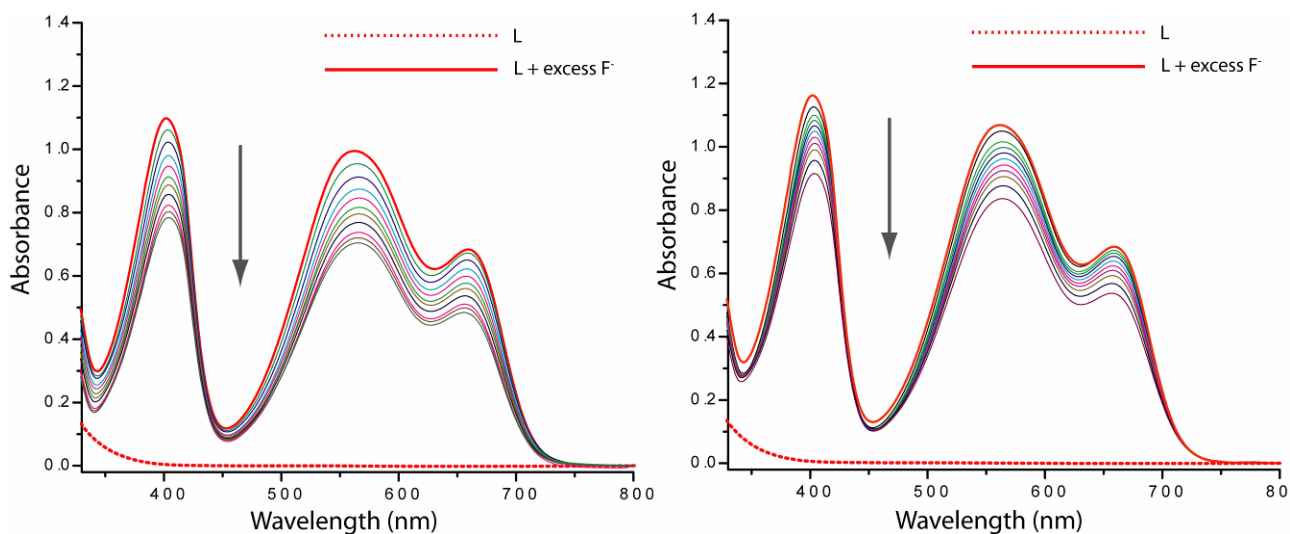


Figure S34. UV-Vis titration curves of **L** (10 μM) charged with excess F^- in dry acetone upon gradual addition of water (left) and methanol (right) upto 1 mL.

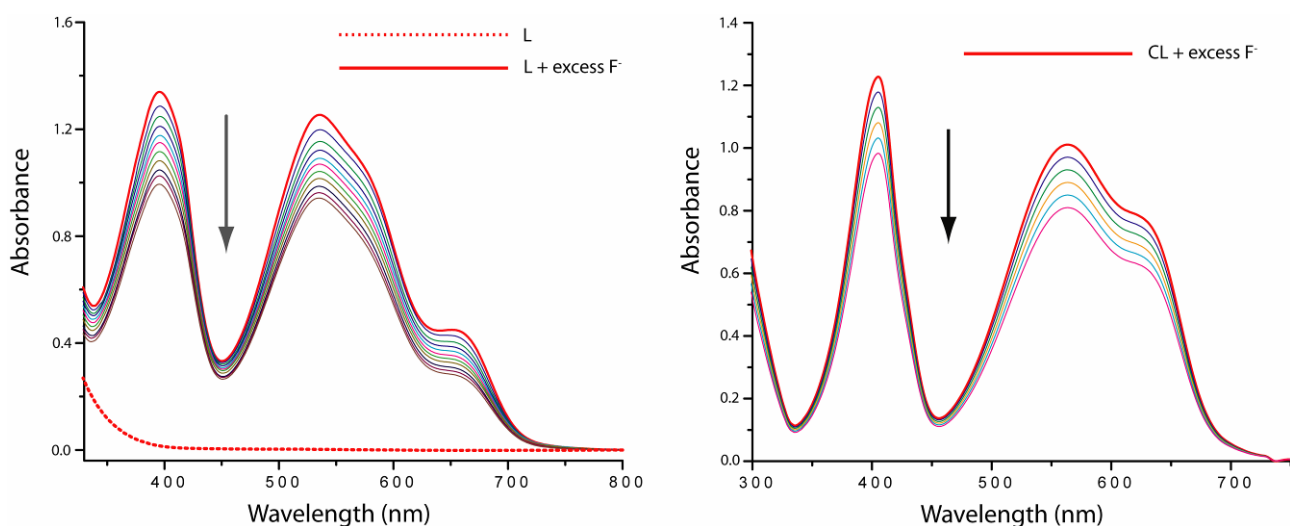


Figure S35. UV-Vis titration curves of **L** (left) and **CL** (right) charged with excess F^- in dry DMSO upon gradual addition of water up to 1 mL.

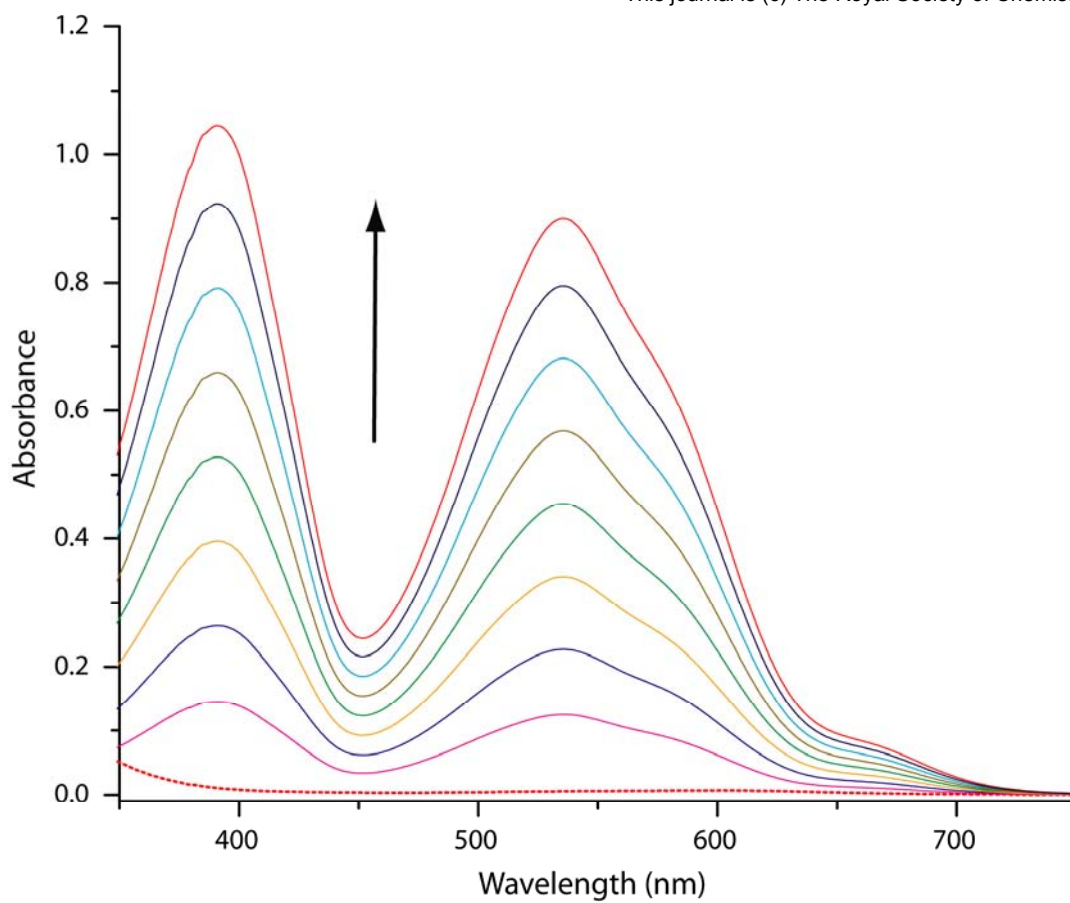


Figure S36. UV-Vis titration curves of **L** (10 μM) in dry DMSO upon increasing addition of standard hydroxide solution (10 mM).

^1H NMR spectra of L in presence of other halides:

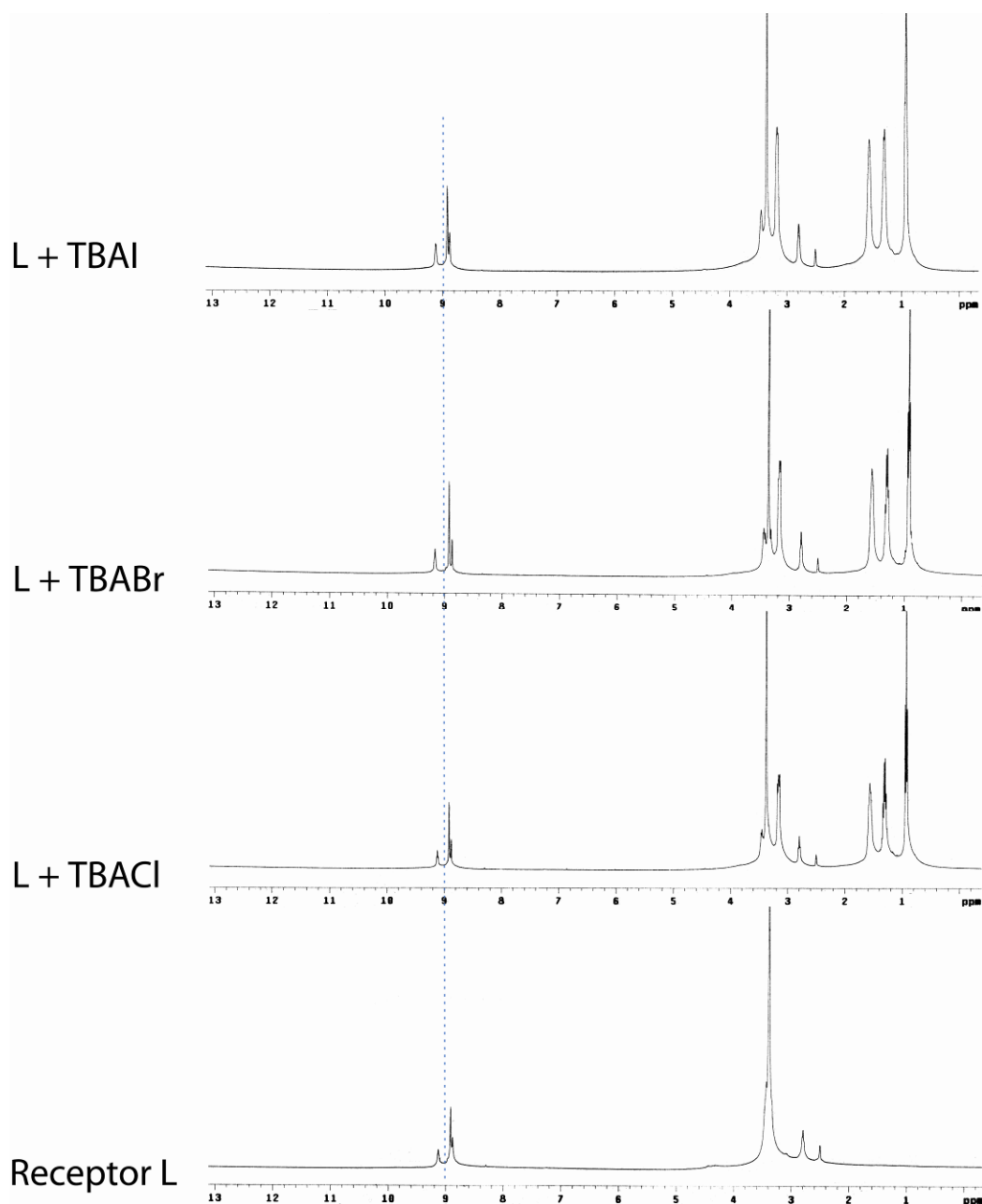


Figure S37. ^1H NMR spectra of L in $\text{DMSO}-d_6$ and upon addition of excess (5 equiv) TBAX (X = Cl, Br, I) at 298 K, showing insignificant shift of the $-\text{NH}$ and aryl $-\text{CH}_a$ protons.

¹H NMR spectra of L in presence of oxoanions:

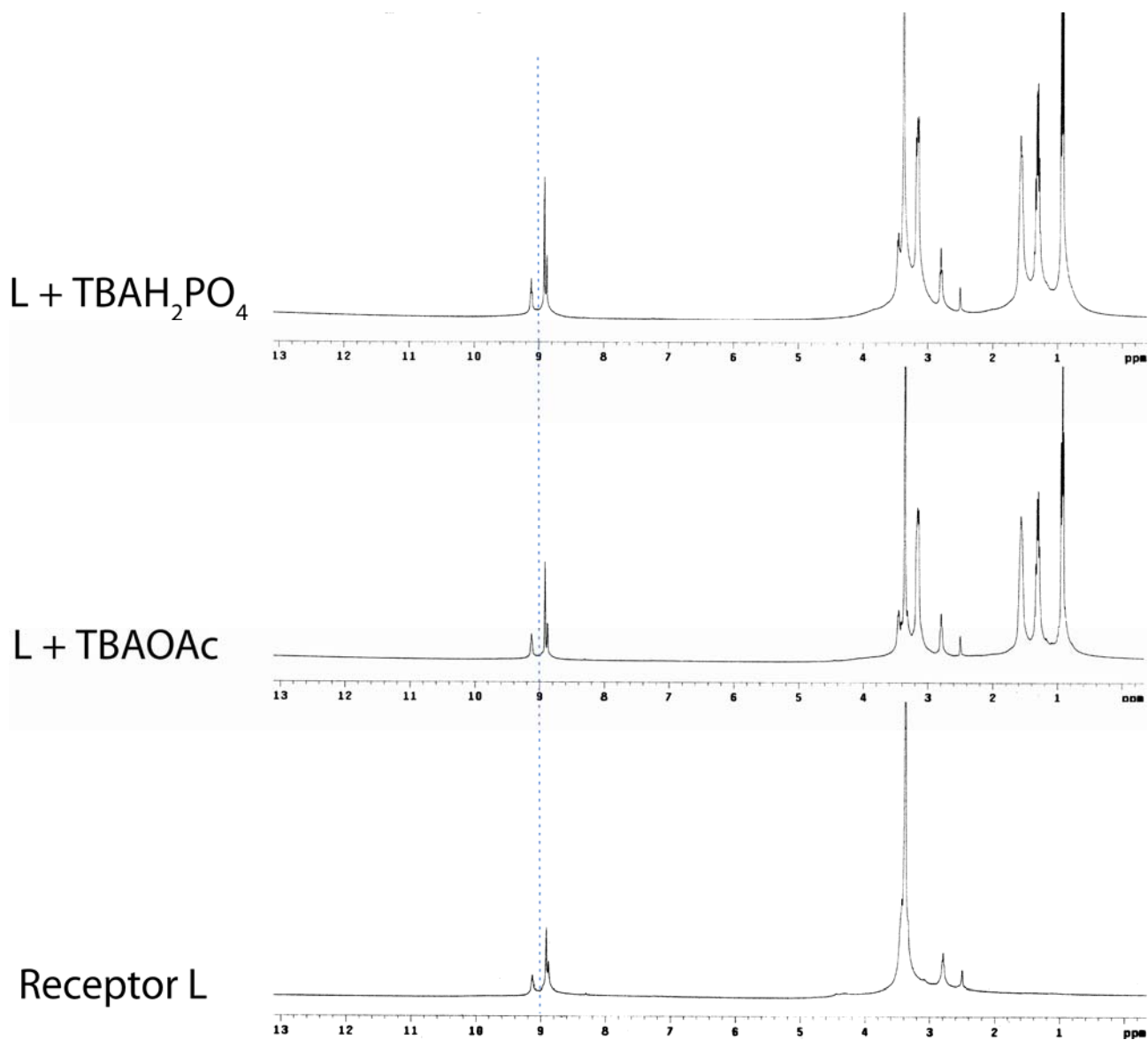


Figure S38. ¹H NMR spectra of L in DMSO-*d*₆ and upon addition of excess (5 equiv) TBAOAc and TBAH₂PO₄ at 298 K, showing insignificant shift of the -NH and aryl -CH_a protons.

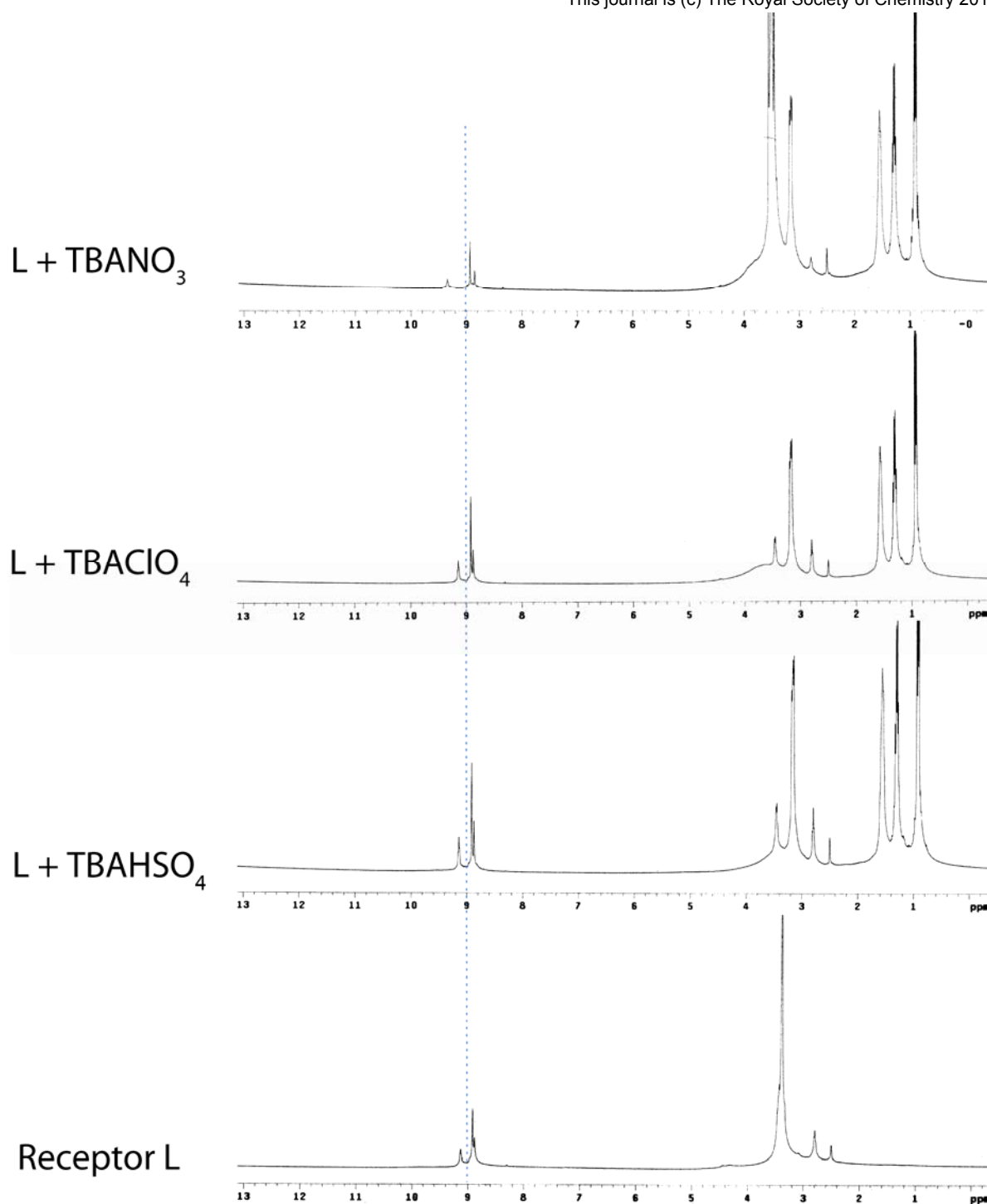


Figure S39. ^1H NMR spectra of **L** in $\text{DMSO}-d_6$ and upon addition of excess (5 equiv) TBAHSO_4 , TBAClO_4 and TBANO_3 at 298 K, showing insignificant shift of the $-\text{NH}$ and aryl $-\text{CH}_a$ protons.

References

- (1) SAINT and *XPREP*, 5.1 ed.; Siemens Industrial Automation Inc.: Madison, WI, 1995. Sheldrick, G. M.
- (2) *SADABS, empirical absorption Correction Program*; University of Göttingen: Göttingen, Germany, 1997.
- (3) Sheldrick, G. M. *SHELXTL Reference Manual: Version 5.1*; Bruker AXS: Madison, WI, 1997.
- (4) Sheldrick, G. M. *SHELXL-97: Program for Crystal Structure Refinement*; University of Göttingen: Göttingen, Germany, 1997.
- (5) Mercury 1.3 Supplied with Cambridge Structural Database; CCDC: Cambridge, U.K., 2003-2004.
- (6) Van der Sluis, P.; Spek, A. L. *Acta Crystallogr.* 1990, A46, 194.